

The Entropy Index (EI): an Auxiliary Tool to Identify the Occurrence of Interplanetary Magnetic Clouds

Ojeda G. A.^{a,c}, Mendes O.^a, Calzadilla M. A.^c, Domingues M. O.^b

^aDGE/CEA/National Institute for Space Research - INPE 12227-010 São José dos Campos, SP, Brazil

^bLAC/CTE/National Institute for Space Research - INPE 12227-010 São José dos Campos, SP, Brazil

^cDepartment of Space Geophysics, Institute of Geophysics and Astronomy - IGA Havana City, Cuba

Abstract

By the study of the dynamical processes related to entropy, this work aims to create a mathematical tool to identify magnetic clouds (MCs) in the interplanetary space using only interplanetary magnetic field (IMF) data. Used as basis for an analysis methodology, the spatio-temporal entropy (STE) measures the image (recurrence plots) “structuredness” in both space and time domains. Initially we worked with the Huttunen et al. 2005’s dataset and studied the 41 MCs presenting a shock wave identified before the cloud. The STE values for each Bx, By, Bz IMF time series, with dimension and time delay equal to one, were respectively calculated. We found higher STE values in the sheaths and zero STE values in some of the three components in most of the MCs (30 among 41 events). In a physically consistent manner, data windows of 2500 magnetic records were selected as the calculation interval for the time series. As not all MCs have zero STE simultaneously, we created a standardization index (an entropy index, called as EI) to allow joining the result of the three components. With the use of EI three not known MCs were indeed identified and then the MVA method allowed calculating their boundaries. Thus the EI is proposed as an auxiliary tool to identify MC candidates based only on IMF analysis. In a promissor condition, this methodology implemented gives basis for an automatic MC identification procedure and surely useful for space weather purposes..

Keywords: space plasmas, space electrodynamics, magnetic cloud, spatio-temporal entropy

1. Introduction

A subset of Interplanetary Coronal Mass Ejections (ICMEs) has simple flux rope-like magnetic fields, which are characterized by enhanced magnetic fields that rotate slowly through a large angle. Such events named magnetic clouds or MCs (Burlaga et al., 1981; Klein and Burlaga, 1982; Gosling, 1990) have received considerable attention because the magnetic field configuration is described by the force-free model (e.g., Lepping et al., 1990; Osherovich and Burlaga, 1997, and references therein). When the MC is moving faster than the surrounding solar wind (SW), the plasma and magnetic field typically accumulate in front of it, forming a disturbed region so-called sheath region. The rapid decrease in the total SW pressure with solar distance is the main driver of the flux-rope radial expansion (Démoulin and Dasso, 2009). However, if a MC is moving slower than the surrounding solar wind (Klein and Burlaga, 1982; Zhang and Burlaga, 1988; Burlaga, 1988), the sheath region is difficult to be detected and the magnetic cloud could go unnoticed by the spacecraft. The shock wave produced by the ICMEs is spatially greater than the magnetic cloud, so a spacecraft can detect only the shock wave sometimes (Schwenn, 2006). Near 1 AU MCs have enormous radial sizes (0.28 AU) with an average duration of 27 h, an average peak of the magnetic field strength of 18 nT and an average solar wind speed of 420 Km/s (Klein and Burlaga, 1982; Lepping and Berdichevsky, 2000). As has been noted by many authors (e.g., Zwickl et al., 1983; Richardson and Cane, 1995), sometimes individual signatures may not be detected in all ICMEs, because they are not present or even there are data gaps.

A practical criterion to detect magnetic clouds is to calculate the plasma beta, defined as the ratio of the thermal and magnetic pressure ($\beta = 2\mu_0 p/B^2$), to find values significantly lower than one. For this calculation, magnetic field and plasma observations at spacecraft are required. Many times the temperature and density data on spacecraft have many gaps during periods in which the plasma instruments could be saturated as a result of intense particle fluxes (for example, Bastille Day in the ACE spacecraft). If this condition occurs, it makes impossible to calculate

22 the plasma beta, but it is still possible to detect the magnetic cloud using magnetometers data (e.g. Huttunen et al.,
23 2005; Nieves-Chinchilla et al., 2005). In this paper, we propose a nonlinear time series analysis as an auxiliary tool
24 to identify magnetic clouds using only the magnetic field data. The result of this calculation can be interpreted as an
25 index related to some dynamical features that identifies the MC.

26 *MC events*

27 MC events were investigated by Huttunen et al. (2005) using the minimum variance analysis (MVA) (Sonnerup and Cahill,
28 1967) to determine if they have a flux-rope structure. They identified 73 MCs in the period (1997 – 2003) and 7 cloud
29 candidate observed by the ACE and WIND spacecraft in solar cycle 23. The axis of a MC can have any orienta-
30 tion with respect to the ecliptic plane (Bothmer and Schwenn, 1994, 1998). This axis orientation, identified by ϕ_C ,
31 the azimuthal direction in the ecliptic, and θ_C , the inclination relative to the ecliptic, is also calculated by the MVA
32 (Bothmer and Schwenn, 1998).

33 To classify MCs, eight flux rope categories are often used:

- 34 – Bipolar MCs (low inclination and flux rope-type: SWN, SEN, NES, NWS), $\theta_C \leq 45^\circ$ and
- 35 – Unipolar MCs (high inclination, and flux rope-type: WNE, ESW, ENW, WSE), $\theta_C > 45^\circ$,

36 where the meanings are S for south, N North, W west and E east.

37 Those authors have also included seven "cloud candidate" events for which either the fitting with MVA was not
38 successful (e.g. the eigenvalue ratio < 2 or the directional change less than 30°) or there was large values of beta
39 throughout the event. In that study the criterion to define a MC were based on the smoothness of the rotation in
40 the magnetic field direction confined to one plane. Additionally, they required that a MC must have the average
41 values of plasma beta less than 0.5, the maximum value of the magnetic field at least 8 nT, and the duration at least
42 6 h. With the last two criteria, they aimed to remove the ambiguity of identifying the small and weak MCs. All
43 selected events were investigated by analyzing 1 h magnetic field data with the MVA (Sonnerup and Cahill, 1967),
44 where MCs are identified from the smooth rotation of the magnetic field vector in the plane of the maximum variance
45 (Klein and Burlaga, 1982).

46 *Nonlinear analysis*

47 The concept of entropy is fundamental for the study of several branches of the physics like statistical mechanics
48 and thermodynamics. Loosely interpreted, entropy is a thermodynamic quantity which describes or quantifies the
49 amount of disorder in a physical system. Therefore we can generalize this concept to characterize or quantify the
50 amount of information stored in more general probability distributions of a time series. This is in part what an
51 information theory is concerned with. The aforementioned theory was developed during the 1940s and 1950s with
52 the main contributions given by Shannon and Weaver (1948); Renyi (1959); Kolmogorov (1958); and Sinai (1959).

53 As the solar wind plasma generates complex fluctuations in a spacecraft-detected signals, those fluctuations can
54 be investigated with techniques adopted from the nonlinear dynamics theory (Remya and Unnikrishnan, 2010). In
55 principle, it is possible to study the MCs by analyzing the time series of interplanetary magnetic field (IMF). So, the
56 main goal in this work is to find some nonlinear tool that helps someone identifying the MCs in the solar wind.

57 Ojeda et al. (2005) studied time series that represent physical parameters of the solar wind (interplanetary magnetic
58 field and velocity components in the plasma flow) recorded by the WIND spacecraft with a time resolution of 1 min.
59 In that work they studied 20 MCs, 17 plasmoids (events not identified as MC), and 20 time series of equivalent time
60 duration of quiet solar wind. The IMF B_z and solar wind V_x components in a time interval of 48 hour before each
61 MC were studied. Under MC conditions, a feature was identified that the IMF B_z has the tendency to present lower
62 spatio-temporal entropy¹ (STE) values than the B_z in other cases, such as in plasmoids and during quiet solar wind. It
63 seems to be a very contrasting aspect to be analyzed. Thus in this work a more detailed study of the STE in MCs is
64 carried out. The behavior of the STE in time series of the IMF components, measured by the ACE spacecraft with a
65 time resolution of 16 s, is explored.

¹name given by Eugene Kononov's Visual Recurrence Analysis (VRA) software, not to be confused with spatio-temporal entropy image (STEI) (Ma and Zhang, 2001)

2. Methodology and Dataset

In this work, the purpose is to present a tool using the STE in a method that can identify simply and quickly the occurrence of a MC at about 1 AU. The main advantage of the approach proposed is that it takes into account only the interplanetary magnetic field data to identify the cloud. Nevertheless, this STE method does not solve the problem of identifying the boundaries of the clouds. To delimit the boundaries, if this is the case, the methodology presented in the work of Huttunen et al. (2005) is available to be used. In order to test and validate our identification methodology, MCs identified by other authors will be also used. Additionally new MCs will be identified by this tool unravelling some features hidden in those time series of data. Our methodology uses a strictly mathematical criterion from the nonlinear dynamics techniques to identify MCs in the solar wind. This methodology is indeed a novelty.

2.1. The recurrence plots in Visual Recurrence Analysis software

It is presented a summary of the ideas expressed in the Eugene Kononov's Visual Recurrence Analysis (VRA) software² about recurrence plots (RPs). In order to present the ideas, some figures are used to guide the description.

Figure 1 shows a RP for a simple sine wave, using the data file just included in VRA software. In it organized patterns of color characteristics are shown for the periodical signal. In order to allow a comparative view, a RP of white noise is shown in Figure 2, with the data file also included. With a different result, an uniform distribution of color characteristics is noticed for the random signal.

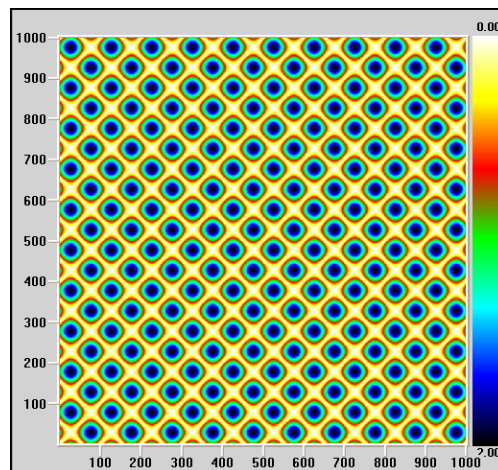


Figure 1: Recurrence plot of simple sine wave, using a data file included with VRA software. In the RP organized patterns of color characteristics are shown for a periodic signal (A color version is available in the electronic version).

The RP is a relatively recent technique for the qualitative assessment of time series (Eckmann et al., 1987), A technique that allow someone detects graphically hidden patterns and structural changes in data or see similarities in patterns across the time series under analysis. The fundamental assumption underlying the idea is that an observable time series (a sequence of observations) is the manifestation of some dynamic process.

It has been proved mathematically that one can recreate a topologically equivalent picture of the original multidimensional system behavior by using the time series of a single observable variable (Takens, 1981). The basic idea is that the effect of all the other (unobserved) variables is already reflected in the series of the observed output. Furthermore, the rules that govern the behavior of the original system can be recovered from its output.

In the RPs a one-dimensional time series from a data file is expanded into a higher-dimensional space, in which the dynamic of the underlying generator takes place. This is done by a technique called "delayed coordinate embedding", which recreates a phase space portrait of the dynamical system under study from a single (scalar) time series. To expand a one-dimensional signal into an M-dimensional phase space, one substitutes each observation in the original

²VRA v4.7 <http://nonlinear.110mb.com/vra/>

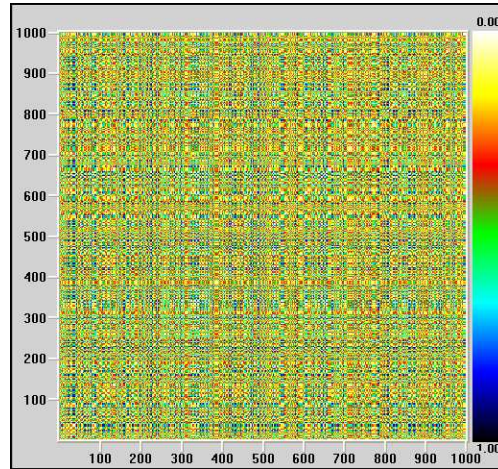


Figure 2: Recurrence plot of White Noise, using data file included with VRA software. In the RP an uniform distribution of color characteristics is shown for a random signal(A color version is available in the electronic version).

94 signal $X(t)$ with vector $(y(i) = \{x(i), x(i-d), x(i-2d), \dots, x(i-(m-1)d)\})$, where i is the time index, m is the embedding
 95 dimension, d is the time delay. As a result, we have a series of vectors $Y = y(1), y(2), y(3), \dots, y(N - (m - 1)d)$, where
 96 N is the length of the original series.

97 With such reconstruction it is possible to reproduce the original system states at each time where we have an ob-
 98 servation of that system output. Each unknown state $Z(t)$ at time t is approximated by a vector of delayed coordinates
 99 $Y(t) = x(t), x(t-d), x(t-2d), \dots, x(t-(m-1)d)$. After the Euclidean distances between all vectors are calculated,
 100 they are mapped to colors from the pre-defined color map and are displayed as colored pixels in their corresponding
 101 places (see Figure 1, for example). The RP is a graphical representation of a correlation integral. The important
 102 distinction (and an advantage) is that the RP, unlike the correlation integrals, preserve the temporal dependence in the
 103 time series, in addition to the spatial dependence.

104 In RPs, if the underlying signal is truly random and has no structure, the distribution of colors is uniform and does
 105 not have any identifiable patterns (see Figure 2, for example). There is some determinism in the signal generator,
 106 which can be detected by some distinctive color distribution. For example, hot colors (yellow, red, and orange) can
 107 be associated with small distances between the vectors, while others colors (blue, black) may be used to show large
 108 distances. In this printed work colors are noticed as a grey pattern (from white to black). Therefore one can visualize
 109 and study the motion of the system trajectories and infer some characteristics of the dynamical system that generated
 110 the time series. Also, the length of diagonal line segments of the same color on the RP brings an idea about the signal
 111 predictability. But, RP is mostly a qualitative tool.

112 For random signals, the uniform (even) distribution of colors over the entire RP is expected. The more determin-
 113 istic the signal, the more structured the RP. So for the purpose of comparison in Figure 1 the RP of a strictly periodic
 114 signal can see and in Figure 2 the RP of the white noise time series.

115 2.2. The entropy concepts in recurrence plot: a review

116 The RP is a visual tool for the investigation of temporal recurrence in phase space (Takens, 1981). In the literature
 117 there are some methods to calculate the entropy in the RP and the phase space (Takens, 1981). The method (STE)
 118 presented by Eugene Kononov's VRA software is the only one provided satisfactory results when it is applied to time
 119 series of the IMF. A brief review on the entropy concepts is presented here.

120 The STE entropy was used to measures the image "structuredness" in a bidimensional representation, *i.e.*, both
 121 in "space" and time domains. It was implemented in VRA software to quantify the order in RPs. In physical terms,
 122 this quantity compares the distribution of distances between all pairs of vectors in the reconstructed state space with
 123 that of distances between different orbits evolving in time. The result is normalized and presented as a percentage
 124 of "maximum" entropy (randomness). When the entropy has a value of 100% it means the absence of any structure

125 whatsoever (uniform distribution of colors, pure randomness, seen in Figure 2). On the other hand, 0% of entropy
 126 implies “perfect” structure (distinct color patterns, perfect “structuredness” and predictability, seen in Figure 1).

127 Recurrence is the most important feature of chaotic systems (Eckmann et al., 1987). The popularity of RPs lies in
 128 the fact that their structures are visually appealing, and that they allow the investigation of high dimensional dynamics
 129 by means of a simple two-dimensional plot (Facchini et al., 2009). For a better understanding and quantification of
 130 the recurrences, Webber and Zbilut (1994) have proposed a set of quantification measures, which are mainly based
 131 on the statistical distribution of the line structures in the RP. Recurrence quantification analysis (RQA) is a nonlinear
 132 technique used to quantify the information supplied by a RP (Webber and Zbilut, 1994; Zbilut and Webber, 1992).
 133 Recurrence variables are calculated from the upper triangular area of the recurrence plot, excluding the central diag-
 134 onal, because the plot is symmetrical about the main diagonal. The RQA can be used as a tool for the exploration of
 135 bifurcation phenomena and dynamics changes also in nonstationary and short time series. The entropy (ENT) is one
 136 of the recurrence variables of the RQA method. It is the Shannon information entropy for the distribution probability
 137 of the diagonal lines. That is:

$$ENT = - \sum_{k=L_{min}, p(k) \neq 0}^{L_{max}} p(k) \log_2(p(k)), \quad (1)$$

138 where L_{min} is the minimum length of diagonal lines in RP and

$$p(k) = \frac{\text{number of diagonal lines of length } k \text{ in RP}}{\text{number of diagonal lines in RP}}. \quad (2)$$

139 The ENT can be calculated using the VRA software; but it should not be confused with the STE.

140 Little et al. (2007) developed a Recurrence Period Density Entropy (RPDE) method, first it requires the embedding
 141 of a time series in phase space, which, according to Taken’s embedding theorems, can be carried out by forming
 142 time-delayed vectors for each value x_n in the time series. Then, around each point in the embedded phase space, a
 143 recurrence neighbourhood of radius ϵ is created. All recurrences into this neighbourhood are tracked, and the time
 144 interval T between recurrences is recorded in a histogram. This histogram is normalized to create an estimate of the
 145 recurrence period density function $p(T)$. The normalized entropy of this density is the RIDE value H_{norm} (Little et al.,
 146 2007).

$$H_{norm} = -(\ln T_{max})^{-1} \sum_{t=1}^{T_{max}} p(t) \ln p(t). \quad (3)$$

147 The RPDE value is a scalar in the range zero to one. For purely periodic signals, $H_{norm} = 0$ (STE=0%) whereas
 148 for purely uniform white noise, $H_{norm} = 1$ (STE=100%). However, estimates obtained with this technique (RPDE)
 149 are different from those obtained with the STE.

150 Dasan et al. (2002) report an analysis, using the tools of nonlinear dynamics and chaos theory, of the fluctuations
 151 in the stress determined from simulations of shear flow of Stokesian suspensions. They also computed the STE using
 152 VRA for the stress. The calculated values of the STE for the shear and normal stresses were nearly zero, show-
 153 ing perfect structure in the data. They observed definite structure in the phase-space plot of the stress components
 154 (Dasan et al., 2002). They cited the works of Peacock (1983); Carr and Schwartz (1998). Peacock (1983) presented
 155 a two-dimensional analogue of Kolmogorov-Smirnov test, useful for analysing the distribution of data in two dimen-
 156 sions, as is the RP. Carr and Schwartz (1998) investigated the fluctuation phenomena in plasmas that often necessitates
 157 the analysis of spatio-temporal signals. It was shown how such signals can be analyzed using the biorthogonal de-
 158 composition, which splits them into orthogonal spatial and temporal modes. Several parameters allow one to quantify
 159 the weight distribution in the biorthogonal decomposition. The total energy of spatio-temporal signal $u(t, j)$ is found
 160 to be equal to the sum of the eigenvalues, α_m :

$$E(u) = \sum_{m=1}^N \alpha_m^2. \quad (4)$$

161 They can define the relative energy of the m^{th} structure as

$$E_m(u) = \frac{\alpha_m^2}{E(u)}, \quad (5)$$

162 and the entropy of the spatio-temporal signal $u(t, j)$ is defined as

$$H(u) = -\frac{1}{\log N} \sum_{m=1}^N E_m(u) \log E_m(u). \quad (6)$$

163 It describes how the energy is distributed across the N_s significant structures. Signal whose energy is concentrated in
 164 a single structure such that $N_s = 1$ will have very low entropy $H(u) = 0$, our $H(u) = 1$ if the energy is distributed
 165 equally among the N_s significant structures.

166 The results will be presented in this paper shows the usefulness of STE implemented by Eugene Kononov's
 167 software. Other ways to calculate the entropy are not useful as an auxiliary tool to identify the occurrence of MCs.

168 2.3. Test of stationary time series using STE

169 From an intuitive point of view, a time series is said to be stationary if there is no systematic change in mean (no
 170 trend) and no systematic change in variance and if strictly periodic variations have been removed (Chartfield, 2003).

171 Trend estimation is a statistical technique to aid in the interpretation of data (Chartfield, 2003). When a time series
 172 related to measurements of a process are treated, trend estimation can be used to make and justify statements about
 173 tendencies in the data. Given a set of data and the desire to produce some kind of "model" of those data (model, in
 174 this case, meaning a function fitted through the data), there are a variety of functions that can be chosen for the fit.
 175 However, if there is no prior understanding of the data, then the simplest function to fit is a straight line and thus this
 176 is the "default". Once it has been decided to fit a straight line, there are various ways to do so, but the most usual
 177 choice is a least-squares fit, equivalent to minimization of the L_2 norm. If there is no global trend in time series the
 178 angle ("trend angle") between the straight line and the positive x axis must be zero, else the angle is not zero. The
 179 aim of this subsection is to calculate the STE versus the trend angle. We deal with time series with data file included
 180 in VRA to calculate the STE of each one versus the trend angle.

181 Figure 3 shows a time series plot of Lorenz data file included in VRA. We gave trends to the series through
 182 rotations about the origin. After that, we calculated the STE of each temporal series. The results were included in
 183 row 2 presented in Table 1, in which three time series with data file included in VRA version 4.7 are shown. The
 effects of the trends in every series related with STE values are quantified.

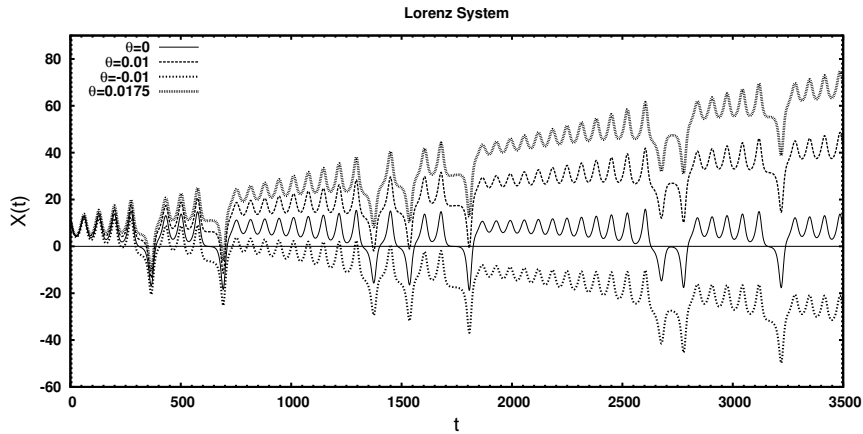


Figure 3: Time series plot of Lorenz data file included in VRA (case with $\theta = 0$). Series rotated about origin ($\theta = -0.01$ rad , $\theta = 0.01$ rad , $\theta = 0.0175$ rad) and the three resulting series also plotted. After that, we calculate the STE of each series.

184 We follow the same idea to cause a trend in time series for another cases, Sine and White Noise data file also
 185 included in VRA. The results were included in rows 3 and 4 of Table 1. For periodic time series (sine data file) the
 186 value of STE is always zero independently from the increasing trend. If the trend in the time series increases, the STE
 187 value decreases (see row 2 and 4 in Table 1).
 188

Table 1: STE values related to trends for three time series with data file included in VRA 4.7.

Series	$\theta = 0$ rad	$\theta = -0.01$ rad	$\theta = 0.01$ rad	$\theta = 0.0175$ rad
STE(Lorenz)	73%	30%	29%	0%
STE(Sine)	0%	0%	0%	0%
STE(White Noise)	80%	34%	34%	3%

189 Also, the first difference applied in a time series is often enough to convert series with a trend into a stationary time
190 series. The first-order differences of time series values $x_1, x_2, x_3, \dots, x_N$ are given by a new series y_1, y_2, \dots, y_{N-1} ,
191 where $y_{N-1} = x_N - x_{N-1}$. The operation $y_t = x_t - x_{t-1} = \nabla x_t$ is called the first difference and ∇ is the difference
192 operator. Sometimes the first differencing is not enough to remove the trend in mean. We then try further differencing.
193 For example, the second-order difference is given by:

$$\nabla^2 y_t = \nabla x_t - \nabla x_{t-1} = x_t - 2x_{t-1} + x_{t-2} \quad (7)$$

194 Our interest is to study variations in the STE values when a first-order differences are applied on stationary time
195 series. In the previously studied time series (Lorenz, Sine and White Noise data file included in VRA), we calculate
196 the first-order differences. After that, we calculated the STE of each time series and compared the results with the STE
197 of the original series, which are shown in Table 2. The STE values are similar in both of them, *i.e.*, for transformed
198 (first-order differences) and untransformed time series. Thus, when the time series has no trend, the non-linear delicate
structures are not destroyed.

Table 2: STE values related to the first-order differences in time series.

Series	Untransformed	first-order differences
STE(Lorenz)	73%	75%
STE(Sine)	0%	0%
STE(White Noise)	80%	82%

199 The entropy value is small and may tend to zero in any time series with trend. The STE value for nonstationary
200 signals is not meaningful. If there is a trend in the time series, you might want to consider removing it by differencing
201 the original time series before calculating the STE. Keep in mind, however, that taking the first differences may destroy
202 the delicate nonlinear structure in the time series (if there is any). Following this idea, sometimes we differentiate the
203 series of the interplanetary magnetic field before calculating the entropy. This is done on a trial basis after calculating
204 the entropy of the original series. The reason is to remove the trend and calculate the true value of entropy of the
205 series, the results are shown in Figure 4 (c) and will be discussed later. The relationship between trend and STE
206 values in magnetic clouds is discussed in this work.
207

208 2.4. ACE spacecraft data

209 The plasma particle detected by ACE arrived to the Earth after approximately 30 min. The Magnetic Field Ex-
210 periment (MAG) on board ACE consists of twin vector fluxgate magnetometers to measure interplanetary magnetic
211 field. The data³ contains time averages of the magnetic field over time periods 1s, 16s, 4min, hourly, daily and 27
212 days (1 Bartels rotation). Magnetic field vectors are given in the RTN, GSE, and GSM coordinate systems. The Solar
213 Wind Electron, Proton, and Alpha Monitor (SWEPAM) measures the solar wind plasma electron and ion fluxes (rates
214 of particle flow) as functions of direction and energy. The data⁴ contains time averages of solar wind parameters over
215 time periods 64s (ion data only), 128s (electron data only), hourly (all data), daily (all data) and 27 days (1 Bartels
216 rotation) (all data).

217 In this paper we use data from the magnetic field components with the time resolution of 16s in GSM and GSE
218 coordinate systems, because we are interested in studying time series of magnetic clouds from 1000 to 5500 data

³http://www.srl.caltech.edu/ACE/ASC/level2/lvl2DATA_MAG.html

⁴http://www.srl.caltech.edu/ACE/ASC/level2/lvl2DATA_SWEPAM.html

219 records. We think that some local informations are lost in the short time series analysis. We cannot calculate the STE
220 in the VRA software for time series with more than 5500 data points (explained later in Subsection 3.1). If we need
221 to detect the boundaries of a magnetic cloud with MVA method then we use data with 1h time resolution (similar to
222 Huttunen et al. (2005)) for MAG and SWEFAM experiments respectively.

223 3. Results and Discussion

224 In the next subsection, we compare STE values between time series corresponding to MCs and sheaths. This
225 comparison is performed only for IMF data, which were data of the MCs detected by Huttunen et al. (2005). From
226 the 73 MCs identified by those researchers we have dealt with just 41 MCs: just for clouds preceded by shock waves.

227 In the other subsections, we have studied time intervals of the solar wind, designated here as solar wind windows,
228 with the purpose of validating a method for detecting MCs. Over all the windows the STE variations were studied.
229 We named the previous methodology of "windowed spatio-temporal entropy". The criteria to select a specific solar
230 wind window are presented in the begin of each subsection.

231 3.1. STE calculated for 41 magnetic clouds between 1998 – 2003

232 We processed ACE data, from March 1998 to December 2003, of the three magnetic field components (B_x , B_y , B_z)
233 in GSM, with a time resolution of 16s. We obtained the recurrence plots for 246 time series ($3 \cdot (41 MCs + 41 Shs) =$
234 246). We have calculated the STE value for each temporal series with embedding dimension and time delay equal
235 to one respectively. It may be noticed that STE value changes for different embedding parameters. For example, for
236 Lorenz attractor (Lorenz data file included in VRA), STE is near its minimum when the correct embedding is used
237 (dimension = 3, time delay = 16 for that particular data file). This and other results suggest that STE can be used
238 to determine the optimal embedding parameters. We selected the same embedding and time delay, equal to one, to
239 maintain equivalence in the calculation of entropy among all series. Table 3 presents the events in chronological order.

240 The STE values for the 41 MC events, presented in Table 3, are shown in Figure 4 (a). At the top, the STE of the
241 three IMF components B_x , B_y and B_z , plotted respectively as the "o", "+" and "x", for the MCs. At the bottom, the
242 same for the sheath regions. In Figure 4 (b), the histogram of STE obtained for the B_z component taking into account
243 the MCs and the sheath regions are shown.

244 In Figure 4 (a), the STE values of the 246 time series (each separated by cloud and sheath respectively) were
245 plotted in chronological order (as appeared in column 1 in Table 3) earlier for MCs and bellow for sheath regions.
246 The STE values were calculated with embedding dimension and time delay equal to one respectively. Some MCs do
247 not have values close to zero entropy in the three components simultaneously. Then, it is possible to find components
248 with perfect structuredness (low STE) and absence of structure (high STE) in the same magnetic cloud.

249 If we compare the STE values between the same components for the sheath and the cloud regions (for example,
250 B_x -sheath ($STE = 56\%$) with STE B_x -cloud ($STE = 0\%$) in the event 1), we detect that for 5/41 (3/41) cases in
251 the B_x (B_y , B_z) component(s) the STE in clouds is bigger than the one in sheath respectively. We found a decrease in
252 entropy in the clouds present in all IMF components. Someone can notice that a clear tendency of the MCs events
253 to present STE with lower values, close to zero, as observed in Ojeda et al. (2005) and extended in this work, which
254 is a new feature added to the usual features (Burlaga et al., 1981) established to the MCs. The STE was zero in
255 20/41, 21/41, 25/41 MCs to B_x , B_y , B_z respectively. The three components had $STE = 0\%$ value in 17/41 MCs and
256 1/41 sheath at the same time. The sheath region with $STE = 0\%$ corresponds to event number 06 in Table 3. The
257 presence of another cloud in the sheath region will be examined later (subsection 3.2.2).

258 Figure 4 (b) shows a histogram of STE derived from (a) for the B_z component of clouds (in grey) and sheaths.
259 We have 37/41 of MCs with STE less than 40% and 37/41 of sheaths with STE greater than 40% respectively. We
260 did some tests with the time series to explain the results above. First, if the Gaussian noise is removed from the
261 signal and the STE calculated, the STE value tend to decrease in less than 5% from its initial value. Second, when
262 a trend is removed of the series through a rotation (with the angle of slope line of best fit) the STE varies, but still
263 the three components had $STE = 0\%$ value in 17/41 MCs and 1/41 sheath at the same time in time series with more
264 than 5500 data points (VRA software limitation). These results are shown in Figure 5 and will be discussed later.
265 Third, by removing the trend through the first order difference in time series (see Figure 4 (c)) we still have MCs with
266 $STE = 0\%$.

Table 3: Solar Wind data studied (from Huttunen et al. (2005)).

No.	Year	Shock	UT	MC, start	UT	MC, stop	UT
01	1998	06 January	13:19	07 January	03:00	08 January	09:00
02		03 February	13:09	04 February	05:00	05 February	14:00
03		04 March	11:03	04 March	15:00	05 March	21:00
04		01 May	21:11	02 May	12:00	03 May	17:00
05		13 June	18:25	14 June	02:00	14 June	24:00
06		19 August	05:30	20 August	08:00	21 August	18:00
07		24 September	23:15	25 September	08:00	26 September	12:00
08		18 October	19:00	19 October	04:00	20 October	06:00
09		08 November	04:20	08 November	23:00	10 November	01:00
10		13 November	00:53	13 November	04:00	14 November	06:00
11	1999	18 February	02:08	18 February	14:00	19 February	11:00
12		16 April	10:47	16 April	20:00	17 April	18:00
13		08 August	17:45	09 August	10:00	10 August	14:00
14	2000	11 February	23:23	12 February	12:00	12 February	24:00
15		20 February	20:57	21 February	14:00	22 February	12:00
16		11 July	11:22	11 July	23:00	13 July	02:00
17		13 July	09:11	13 July	15:00	13 July	24:00
18		15 July	14:18	15 July	19:00	16 July	12:00
19		28 July	05:53	28 July	18:00	29 July	10:00
20		10 August	04:07	10 August	20:00	11 August	08:00
21		11 August	18:19	12 August	05:00	13 August	02:00
22		17 September	17:00	17 September	23:00	18 September	14:00
23		02 October	23:58	03 October	15:00	04 October	14:00
24		12 October	21:36	13 October	17:00	14 October	13:00
25		28 October	09:01	28 October	24:00	29 October	23:00
26		06 November	09:08	06 November	22:00	07 November	15:00
27	2001	19 March	10:12	19 March	22:00	21 March	23:00
28		27 March	17:02	27 March	22:00	28 March	05:00
29		11 April	15:18	12 April	10:00	13 April	06:00
30		21 April	15:06	21 April	23:00	22 April	24:00
31		28 April	04:31	28 April	24:00	29 April	13:00
32		27 May	14:17	28 May	11:00	29 May	06:00
33		31 October	12:53	31 October	22:00	02 November	04:00
34	2002	23 March	10:53	24 March	10:00	25 March	12:00
35		17 April	10:20	17 April	24:00	19 April	01:00
36		18 May	19:44	19 May	04:00	19 May	22:00
37		01 August	23:10	02 August	06:00	02 August	22:00
38		30 September	07:55	30 September	23:00	01 October	15:00
39	2003	20 March	04:20	20 March	13:00	20 March	22:00
40		17 August	13:41	18 August	06:00	19 August	11:00
41		20 November	07:27	20 November	11:00	21 November	01:00

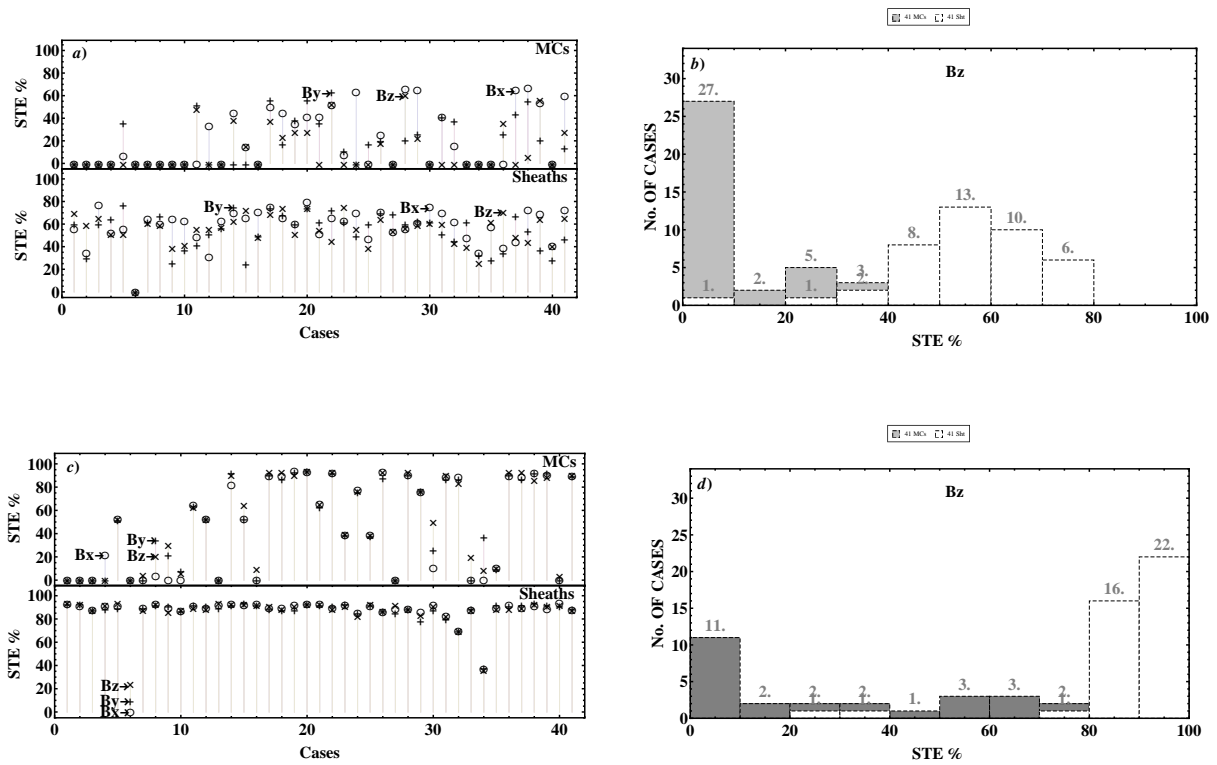


Figure 4: (a) The STE values for the 41 MC events between 1998-2003 presented in Table 3. At the top, the STE for B_x , B_y and B_z , the three IMF components, plotted respectively as the "o", "+" and "x". At bottom, the same as to above but for the sheath regions. (b) The histogram of STE obtained from (a) for the B_z component taking into account the cloud and the sheath regions. (c) It is similar to (a), but with the trend removed through the first-order differences in time series. (d) It is similar to (b), The histogram of STE obtained from (c) for the B_z component taking into account the cloud and the sheath regions.

267 Figure 4 (c) is similar to panel (a), but we have eliminated the trend through the first order difference in time series.
 268 In this case most of the STE values in the sheath increased to $\sim 90\%$ in the three components. Figure 4 (d) shows a
 269 histogram of STE derived from (c) for the B_z component of clouds and sheaths. If we eliminate the trend in the series
 270 then the entropy increases. Then, there is not a nonlinear structure in the time series, the signal is nondeterministic.
 271 Also the STE increases in the clouds, but there are still MCs with zero STE. We find a limitation to interpret this case,
 272 the length of the series. The calculation of the STE with the VRA software, version 4.7, can not be made for time
 273 series with a size bigger than 5500 points because the STE results always in zero. It seems to be a limitation of the
 274 software by some reason not explained in its tutorial.

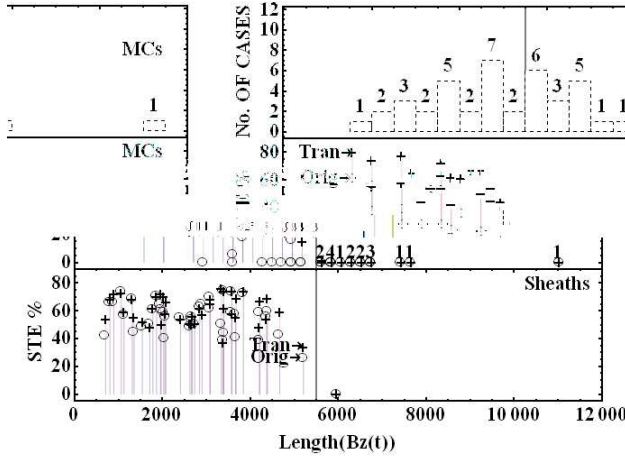


Figure 5: At middle, STE values versus time series length for B_z component for the 41 MCs, where the "o" and "+" symbols corresponds to original and transformed (remove the Gaussian noise and trend through a rotation) time series respectively. At bottom STE values versus time series length for the 41 sheaths. At top the number of events versus intervals of the time series length. The histogram helps to identify overlapping points of MC in the middle panel. The STE is zero to the right of the vertical line due to a software limitation.

275 In Figure 5 at bottom, we have plotted the STE versus the length of the time series for the B_z components for a
 276 sheath region. The "o" and "+" symbols correspond respectively to the original and transformed (by removing the
 277 Gaussian noise and "trend" through a rotation) time series. Panel at middle is similar to one at bottom but for the MC
 278 region. The numbers to the right of the vertical line show the total of events (17) that each point represent. At top, the
 279 histogram helps to identify overlapping points of MC in the middle panel. The STE is zero to the right of the
 280 vertical line due to a software limitation. At middle panel, we have MCs ("o" symbols or original) with zero STE values to
 281 the left of the vertical line. When we remove the Gaussian noise and trend through a rotation the STE values ("+"
 282 symbols or transformed) increase and are different from zero.

283 In Figure 5, related to the top and middle plots, it is shown $STE = 0\%$ in 17/41 (events 1 – 4, 6 – 10, 13, 16, 27,
 284 30, 33 – 35, 40 in Table 3) in the MC with more than 5500 points, in the other 9/41 MCs (events 5, 12, 21, 23 – 25,
 285 31, 32, 37 in Table 3) the STE value leaves the zero value when the time series were transformed by removing the
 286 Gaussian noise and "trend" through a rotation. So far, we have been seeking the causes of the large amount of MCs
 287 with $STE = 0\%$. During a MC, the magnetic field strength is higher than the average, the magnetic field direction
 288 rotates smoothly through a large angle, then the periods with MCs present more trend in the magnetic behavior than
 289 the periods of sheaths or "quiet" solar wind. The trend is the principal cause of the lower STE values in MC. Also, the
 290 MCs are more structured than sheath and "quiet" solar wind (Ojeda et al., 2005). Then it establishes a new feature to
 291 be considered in analyses.

292 3.2. The Windowed Spatio-Temporal Entropy

293 From the 41 MCs studied the STE decreases inside the MCs in relation to the sheath. In Ojeda et al. (2005) we
 294 found MCs with lower STE values than the "quiet" solar wind and other events in the interplanetary medium not
 295 identified as MCs. Then we have decided to analyze solar wind intervals of 10 days where we already knew about the
 296 existence of MCs, as the events reported in Table 3. As a criterion we have selected data windows of 2500 records

297 moving forward as 200 records at head, until the end of the time series was reached. For every data segment selected
 298 the STE was calculated, allowing to analyze the evolution of the STE at every $200 * 16s$ in time evolution for every
 299 2500 records in the time series.

300 We select 2500 points because this interval represents an interval of 11.11 h, and the MCs have a smooth rotation
 301 of the magnetic field vector in the order of 1 day, where the field reaches a peak and decreases. With a temporal
 302 window size of 11.11 h and a resolution of 16 s it is possible to cover the entire range of trend in the most of
 303 MCs with dimensions larger than 24 h. The STE values are calculated every 0.89 h (STE time resolution adopted) and
 304 representing $\sim 8\%$ of the size of each temporal window. So the variation of the values of STE between two continuous
 305 windows (11.11 h) must also be in the order of $\sim \pm 8\%$, a sufficient condition for our initial purpose. We will be able
 306 to study in detail the calculation of the STE by temporal windows for six solar wind intervals following in the studies
 307 (4 MCs represented in Table 3 and other 2 cases).

3.2.1. 07-January-1998 MC event

308 We decided to study in more details the STE variations taking into account some days before and after the event
 309 number 1 in the Table 3. The time series of the B_x , B_y and B_z IMF components of MC has zero STE value (see, Fig-
 310 ure 4 (a), the first event). We find in Figure 5 that the time series are composed of 6753 data points and, consequently,
 311 we have zero entropy when the STE was calculated using the VRA software.

312 Based on the features analyzed in the beginning of this section, our hypothesis is to find zero STE in the period of
 313 the magnetic cloud to identify it. Then, we have selected a time window for 03 – 12 January, 1998 and take IMF three
 314 components in the Geocentric Solar Magnetospheric (GSM) coordinate system recorded by the ACE spacecraft with
 315 time resolution of 16s. We selected data windows of 2500 records moving forward as 200 records to head, until the
 316 end of the time series. The numbers of windows result in 258 and we calculate the STE of each one.

317 In Figure 6, we show the values of STE versus time for the time series of IMF B_x , B_y and B_z components in the
 318 solar wind. Additionally, we investigated if ACE detected some other event during these ten days.
 319

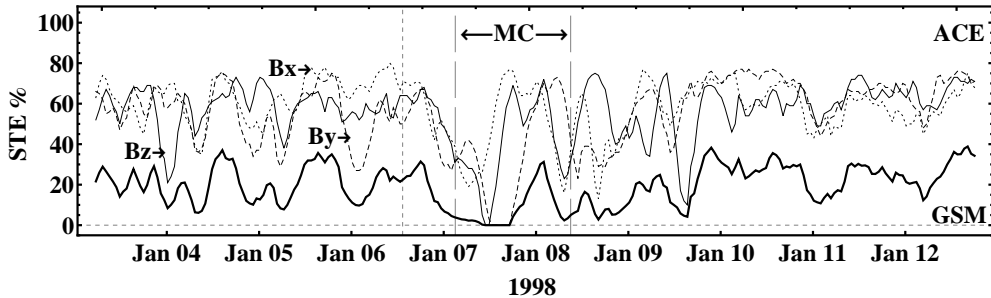


Figure 6: Values of spatio-temporal entropy on January 03 – 12, 1998, as a function of the time for times series of IMF B_x , B_y and B_z components in the solar wind. The thick curve represents the Entropy Index (EI) calculated over the analyzed period. The shock, the start and end of the MC are represented by three vertical dotted lines.

320 Cane and Richardson (2003) summarized the occurrence of interplanetary coronal mass ejections (ICMEs) in the
 321 near-Earth solar wind during 1996 – 2002, corresponding to the increasing and maximum phases of solar cycle 23.
 322 In particular, they give a detailed list of such events based on in situ observations. They reported two ICME in this
 323 interval, 07 January 01 : 00 to 08 January 22 : 00 and 09 January 07 : 00 to 10 January 08 : 00. Then we have one
 324 MC, one interplanetary disturbance that was not classified as MC, and a "quiet" solar wind period. Some features
 325 related to the ICME classified as MC in January 07 were reported by Cane and Richardson (2003): for example
 326 $V_{ICME} = 400km/s$ is the mean solar wind speed in the ICME; $V_{max} = 410km/s$ is the maximum solar wind speed in
 327 the post disturbance region; $B = 16nT$ is the mean field strength; $V_T = 480km/s$ is the transit speed. The MC was
 328 also reported by Huttunen et al. (2005) but with different size (see Table. 3).

329 We used the dates reported by Huttunen et al. (2005) to represent the shock, the start and end of the MC. These
 330 dates were represented with three vertical dotted lines in Figure 6. This unipolar MC has a flux-rope type ENW

331 and the observed angular variation of magnetic field is left-handed (Huttunen et al., 2005). The MVA method gives
 332 the eigenvalue ratio $\lambda_2/\lambda_3 = 48$, the angle between the first and the last magnetic field vectors $\chi = 160^\circ$, and the
 333 orientation of the axis $(\phi_C, \theta_C) = (21^\circ, 52^\circ)$. The B_z component was northward almost during the whole passage of
 334 the MC, then a magnetic storm ($Dst_{min} = -77nT$) is caused by the sheath of heated and compressed solar wind plasma
 335 piled up in front of CME ejecta (Tsurutani et al., 1988).

336 Figure 6 shows the behavior of STE in ten days of solar wind. The B_y , B_z components have a zero STE value
 337 only during the passage of the MC, approximately in the first half of it. The second minimum value of $STE = 10\%$
 338 corresponds to B_z component in January, 09. At this date (09 Jan 07 : 00 – 10 Jan 08 : 00) Cane and Richardson (2003)
 339 detected one ICME with $V_{ICME} = 450Km/s$, $V_{max} = 500Km/s$, $B = 6nT$. This result seems to be very interesting
 340 because in ten days of solar wind data two magnetic components had zero value only within a MC. Huttunen et al.
 341 (2005) first performed a visual inspection of the data to find the candidate MCs. This is always the first step in any
 342 work aiming at studying magnetic clouds. Then, the calculation of STE could be used as a mathematical tool to help
 343 finding the candidate MCs and being a new feature of many MCs. To generalize this idea it is necessary to study
 344 other MCs and explain physically two questions: (1) Why STE is zero only somewhere inside the MC? (2) Why don't
 345 all the magnetic components have zero STE inside the MC? These questions will be answered later. As not all the
 346 magnetic components have zero entropy at the same time, we created a standardization index (called by us Entropy
 347 Index (EI)) to allow joining the results of the three variable (B_x, B_y, B_z) based on the physical process related to the
 348 MC geometry. The index is the result of multiplying the values of entropy of the three variables at the same time t
 349 normalized by 10^4 :

$$EI = \prod_{i=1}^3 \frac{STE}{10^4} [\%] \quad (8)$$

350 The thick curve in Figure 6 is the representation of the EI calculated over the analyzed period. We could think
 351 of a similarity with the Dst index, which is a geomagnetic index which monitors the world wide magnetic storm
 352 level. Negative Dst values indicate that a magnetic storm is in progress, the more negative Dst, the more intense the
 353 magnetic storm. But the entropy index value can only decrease to zero somewhere inside the MC. The MCs have
 354 simple flux rope-like magnetic fields, characterized by enhanced magnetic fields that rotate slowly through a large
 355 angle. Then, the time series of IMF components have a trend and a more ordered dynamic behavior and a higher
 356 degree of correlation between its temporary neighbors (Ojeda et al., 2005). The above mentioned behavior is found
 357 only in the magnetic structures of the MCs, a necessary condition for the zero entropy index value. Conclusion, using
 358 the entropy index we find the MC occurrences. But not the frontiers.

359 3.2.2. 20-August-1998 MC event

360 We take this temporal windows of ten days because we already knew that there was an MC near the center, as
 361 reported in Table 3 number 6 event. Also, this is the only event that has zero STE in the sheath.

362 Figure 7 is similar to Figure 6 but in the period 15 – 25 August 1998. At this date (19 Aug 18 : 47 – 21 Aug 20 :
 363 00, 1998), Cane and Richardson (2003) detected one ICME classified as MC with $V_{ICME} = 300Km/s$, $V_{max} =$
 364 $340Km/s$, $B = 14nT$. The three numbered (1, 2, 3) vertical dotted lines in Figure 7 represent the shock (1), the
 365 start (2) and end (3) of the MC2 reported by Huttunen et al. (2005) (see event number 6 Table 3). The MVA method
 366 to MC2 gives $\lambda_2/\lambda_3 = 30$, $\chi = 177^\circ$ and $(\phi_C, \theta_C) = (113^\circ, -16^\circ)$. This bipolar MC has a flux-rope type SWN and
 367 the observed angular variation of the magnetic field is right-handed (Huttunen et al., 2005). The observed SN-type
 368 MC had $B_z < 0$ for about eleven hours, with values of less than $-10nT$. In the sheath it was observed $B_z < 0$
 369 for more than seven hours and values close to $B_z = -11nT$. The Dst index shows two geomagnetic storms, the first with
 370 $Dst_{min} = -42nT$ caused by the sheath, the second with $Dst_{min} = -67nT$ caused by the MC.

371 Figure 7 shows that the B_x , B_y components have a zero STE value during the sheath of the MC, approximately
 372 at the end half of it. After that, approximately in the center of the MC, the three components (B_x , B_y , B_z) have zero
 373 STE values. The EI is zero at the end of the sheath and within the MC. We think that maybe there are two magnetic
 374 clouds, one after the other. It is very difficult to detect the two MCs when a visual inspection of the data is performed
 375 and then apply the method of minimum variation (see Bothmer and Schwenn, 1998). Someone could make a mistake
 376 in the interpretation of the cloud considering it as part of the sheath of the other MC. To solve the above hypothesis,
 377 we used the same method (MVA) explained in Huttunen et al. (2005), with success.

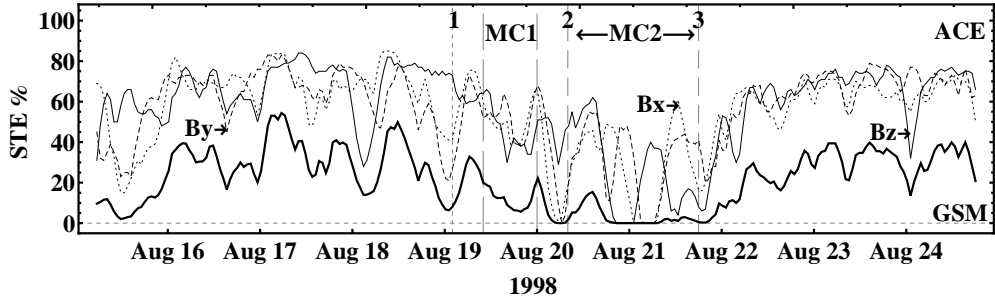


Figure 7: Values of Spatio-Temporal Entropy on 15 – 25 August, 1998 as a function of the time for times series of IMF B_x , B_y and B_z components in the solar wind. The thick curve represents the Entropy Index (EI) calculated over the analyzed period. We identify the MC1. EI is zero after the cloud due to the adjustment in the time window for calculating the entropy and that this cloud is small.

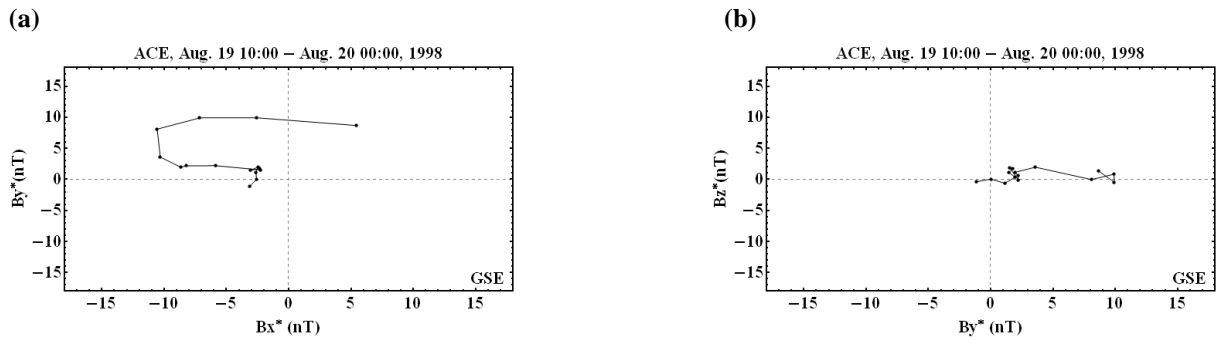


Figure 8: The rotation of the magnetic field vector in the plane of maximum variance and in the plane of minimum variance for the bipolar MC observed by ACE on 19 August at 10:00 UT to 20 August at 00:00 UT 1998. In the Figure 7 shown this MC (MC1), the EI help to identify the MC.

378 On 19 August 1998, at 02 : 00 UT the parameters were: proton density $N_p = 3.57 \text{ cm}^{-3}$, the proton temperature
 379 $T_p = 7.31 * 10^4 \text{ K}$, the ratio of *alphas/protons* = $4.5 * 10^{-3}$, the proton speed $V_p = 333.9 \text{ km/s}$, magnetic field
 380 magnitude $B = 2.4 \text{ nT}$ and plasma beta $\beta = 1.6$. One hour later some parameters had a change to $N_p = 3.98 \text{ cm}^{-3}$,
 381 $T_p = 7.1 * 10^4 \text{ K}$, *alphas/protons* = $6.1 * 10^{-3}$, $V_p = 331.1 \text{ km/s}$, $B = 0.57 \text{ nT}$ and $\beta = 29.8$. It is very difficult to
 382 identify a shock, but the plasma beta increased abruptly and we believe it was related to the arrival of an event. Two
 383 hours later, at 05 : 00 UT, the plasma beta decreased to $\beta = 0.58$, after that there were eleven hours with gaps. The
 384 plasma beta minimum value was $\beta = 7.8 * 10^{-2}$ at 21 : 00 UT where there was a maximum magnetic field magnitude
 385 of $B = 13.3 \text{ nT}$. We used the magnetic field rotation confined to one plane, the plane of maximum variance ($B_x^* B_y^*$)
 386 (see Figure 8), to find the boundaries of the cloud.

387 Finally, we identified the bipolar MC1 observed by ACE on 19 August at 10 : 00 UT to 20 August at 00 : 00
 388 UT (see Figure 8). This MC has a flux-rope type SEN and the observed angular variation of the magnetic field is
 389 left-handed. The MVA method gives to MC1 the eigenvalue ratio $\lambda_2/\lambda_3 = 18$, the angle between the first and the
 390 last magnetic field vectors $\chi = 142^\circ$, the orientation of the axis $(\phi_C, \theta_C) = (135^\circ, 19^\circ)$, the direction of minimum
 391 variance $(\phi_{min}, \theta_{min}) = (43^\circ, -6^\circ)$ and eigenvalues $[\lambda_1, \lambda_2, \lambda_3] = [15.9, 12.6, 0.7]$. In Table 4 we show the date of the
 392 two MCs, the time between the first and second MC is $8h$ (sheath of the second MC). The minimum speed in the first
 393 MC (MC1) was $V_{p1} = 272.9 \text{ km/s}$ at 15 : 00 UT and in the beginning of the second MC (MC2) the maximum speed
 394 was $V_{p2} = 346.1 \text{ km/s}$ one day later, at 05 : 00 UT. Then, $V_{p2} > V_{p1}$ and the two events are very close to each other.
 395 Probably there are other similar cases where a MC was confused within the sheath of the preceding MC. The entropy
 index (EI) can help to identify the MCs and such kinds of cases and find the boundary of MC with MVA method.

Table 4: Two continues MCs from 19 – 21 August 1998. The EI helps to identify the first MC.

Year	Shock1	MC1, start	MC1, stop	MC2, start	MC2, stop
1998	19 Aug, 02:00	19 Aug, 10:00	20 Aug, 00:00	20 Aug, 08:00	21 Aug, 18:00

396

3.2.3. 18-February-1999 MC event

397 A study in more details of the STE variations is presented for some days before and after the event number 11
 398 Tabla 3. Time series of the magnetic components B_x , B_y and B_z for MC have nonzero STE values (see, Figure 4a, the
 399 eleventh point). Why is this happening? To answer this question we calculate the windowed STE of three magnetic
 400 components B_x , B_y and B_z in windows temporal of ten days.

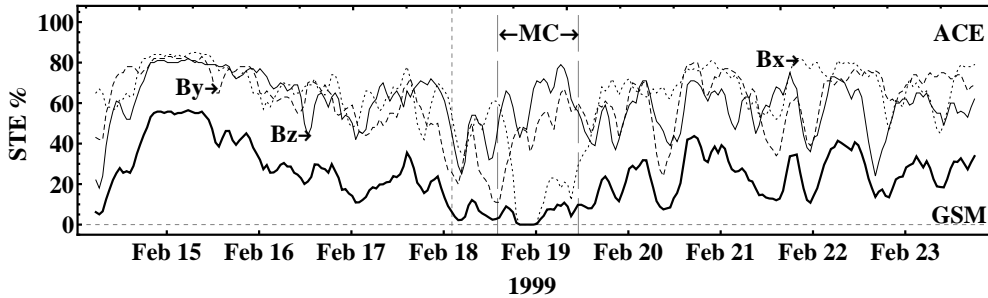


Figure 9: Values of spatio-temporal entropy at 14 – 24 February, 1999 as a function of the time for times series of IMF B_x , B_y and B_z components in the solar wind. The thick curve represents the Entropy Index (EI) calculated over the analyzed period.

401

402 Cane and Richardson (2003) detected one ICME not classified as MC at the date 13 Feb 19 : 00 - 14 Feb 15 : 00
 403 1999 with $V_{ICME} = 440 \text{ km/s}$, $V_{max} = 470 \text{ km/s}$ and $B = 9 \text{ nT}$. Figure 9 shows the results of the calculation
 404 of STE from 14 Feb 15 : 00 1999 and the EI has a small but non-zero value. At the date 18 – 21 Feb 1999 the
 405 ACE spacecraft detected one ICME classified as MC with $V_{ICME} = 520 \text{ km/s}$, $V_{max} = 700 \text{ km/s}$, $B = 8 \text{ nT}$ and
 406 $V_T = 870 \text{ km/s}$ was the transit speed (Cane and Richardson, 2003). The MVA method gives $\lambda_2/\lambda_3 = 8$, $\chi = 83^\circ$ and

407 $(\phi_C, \theta_C) = (96^\circ, 6^\circ)$. This bipolar MC has a flux-rope type NWS and the observed angular variation of magnetic field
 408 is left-handed (Huttunen et al., 2005). Inside the MC represented by vertical lines in the Figure 9, one can see that the
 409 $STE = 0\%$ only for the B_x component. In this case, during the analyzed 10 days the $EI = 0\%$ only inside the MC.

410 So far, we see MCs with zero values of STE only in one component, in two or three at a time. The interpretation
 411 is that it may be related to the inclination of the axis of the MC relative to the ecliptic plane and the distance from the
 412 spacecraft to the axis, but we have poor statistics and this issue remains open. However, the EI has always detected
 413 the presence of a magnetic cloud.

414 3.2.4. 13-October-2000 MC event

415 It is presented a study in more details of the STE variations with some days before and after the event number 24
 416 Tabla 3. Time series of the magnetic components B_y and B_z for MC have zero STE (see, Figure 4a the twenty-fourth
 417 point) but B_x has nonzero STE.

418 Figure 10 shows the results of the calculation of STE from 8 – 18 October 2000. On October 8 the B_x , B_y ,
 419 components had small values of STE but different from zero. At this date it was not reported the presence of ICME,
 420 but we saw a small magnetic structure where the field had a smooth variation. The EI detects these small structures
 that are unnoticed in most of the studies.

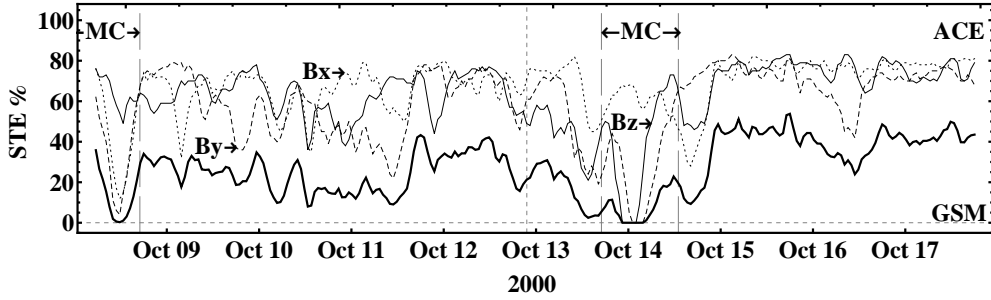


Figure 10: We show the values of spatio-temporal entropy on 08 – 18 October, 2000 as a function of the time for times series of IMF B_x , B_y and B_z components in the solar wind. The thick curve is the calculation of Entropy Index (EI) over the analyzed period.

421 In the Figure 11 (a) solar wind parameters during one MC event are shown. From top to bottom: magnetic field
 422 strength, polar (B_{lat}) and azimuthal (B_{long}) angles of the magnetic field vector in GSE coordinate system, solar wind
 423 speed and plasma beta. The first vertical line indicate the shock, the other two vertical lines indicate the interval of
 424 a MC. The plasma beta minimum value were $\beta = 2.7 \times 10^{-3}$ on 07 October at 23 : 00 UT. We used the magnetic
 425 field rotation confined to one plane, the plane of maximum variance ($B_x^* B_y^*$) to find the boundaries of the cloud (see
 426 Table 5). The MVA method gives the eigenvalue ratio $\lambda_2/\lambda_3 = 47.5$, the angle between the first and the last magnetic
 427 field vectors $\chi = 148.4^\circ$, the orientation of the axis $(\phi_C, \theta_C) = (113.8^\circ, 7^\circ)$, the direction of minimum variance
 428 $(\phi_{min}, \theta_{min}) = (22^\circ, -10^\circ)$ and eigenvalues $[\lambda_1, \lambda_2, \lambda_3] = [124.6, 41.8, 0.9]$. This MC has a flux-rope type SEN (see
 429 panel two and three in Figure 11 (a)) and the observed angular variation of the magnetic field is left-handed.

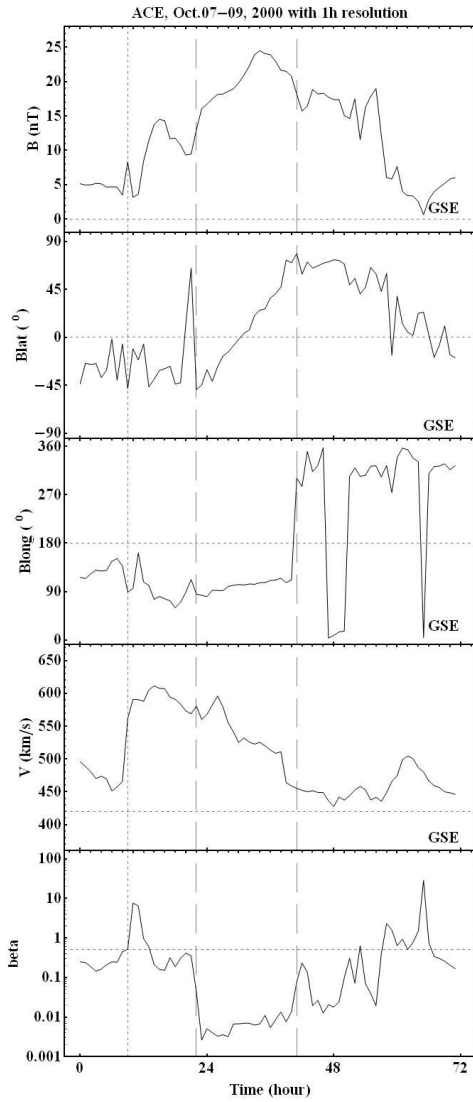
430 Cane and Richardson (2003) detected one ICME classified as MC in the date 12 October 22 : 28 - 14 October
 431 17 : 00 2000 with $V_{ICME} = 410 km/s$, $V_{max} = 470 km/s$, $B = 13 nT$ and $V_T = 580 km/s$. The MVA method gives
 432 $\lambda_2/\lambda_3 = 4$, $\chi = 62^\circ$ and $(\phi_C, \theta_C) = (33^\circ, -25^\circ)$. This bipolar MC has a flux-rope type NES and the observed angular
 433 variation of magnetic field is right-handed (Huttunen et al., 2005). The B_y , B_z components have $STE = 0\%$ only
 434 during the passage of the MC, approximately in the first half of it and the EI detected the presence of the MC.

Table 5: Magnetic Cloud from 07 – 08 October 2000.

Year	Shock	MC, start	MC, stop
2000	07 October, 09 : 00	07 October, 22 : 00	08 October, 17 : 00

435

(a)



(b)

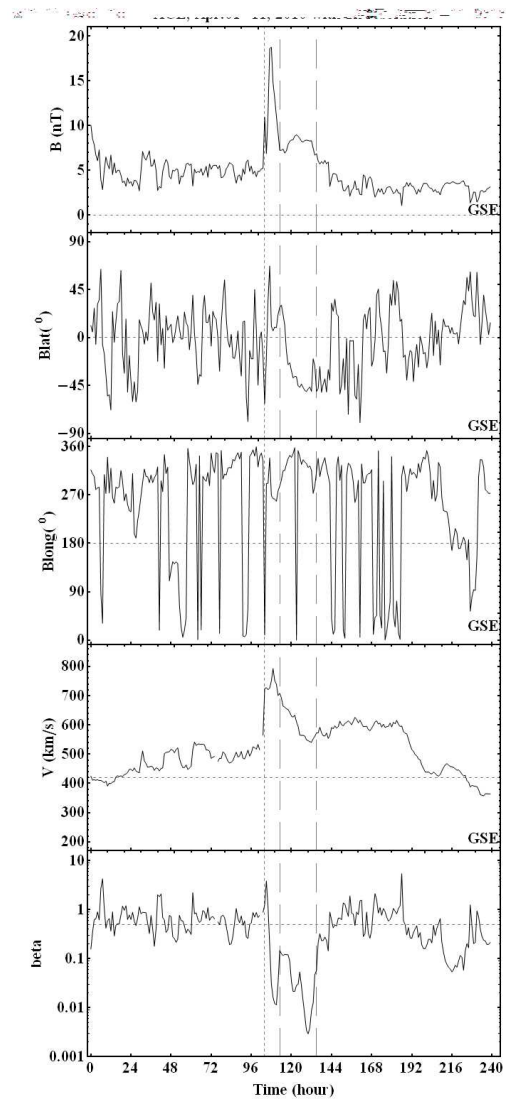


Figure 11: Left and right part : Solar wind parameters during two MC events. Top to bottom: magnetic field strength, polar (Blat) and azimuthal (Blong) angles of the magnetic field vector in GSE coordinate system, solar wind speed and plasma beta. The first vertical line indicate the shock, the other two vertical lines indicate the interval of a MC. Left: 07 – 09 October 2000, the bipolar MC observed by ACE on 07 October at 22 : 00 UT to 08 October at 17 : 00 UT 2000. Right: 01 – 11 April 2010, the bipolar MC observed by ACE on 05 April at 16 : 00 UT to 06 April at 14 : 00 UT 2010.

436 *3.2.5. Interface between the interplanetary ejecta and the high-speed stream on 22 October 1999*

437 High-speed streams, originating in coronal holes, are observed often following interplanetary coronal mass ejection (ICME) at 1 AU (Klein and Burlaga, 1982). Dal Lago et al. (2006) studied the 17 – 22 October (1999) solar-interplanetary event, which was associated to a very intense magnetic storm ($Dst = -237$ nT). They presented an analysis of pressure balance between the ICME observed on 21 – 22 October and the high-speed streams following this ICME. Close to the Earth, at $L1$, an interplanetary shock was detected by ACE magnetic field and plasma instruments on 21 October (1999), at 01 : 34 UT, as shown in Figure 12 with the first vertical dotted line. The driver of this shock is an ICME, which can be distinguished from the normal solar wind by its intense magnetic field, of the order of 20 nT throughout the most part of 21 October, and its low beta (~ 0.1) (Dal Lago et al., 2006). The start of the ejecta was at 03 : 58 UT of 21 October. Toward the end of this ejecta, an increase of the magnetic field intensity was observed, starting at 02 : 30 UT of 22 October, reaching a peak value of 37 nT (Dal Lago et al., 2006). At 06 : 15 UT of 22 October (the second vertical dotted line in Figure 12), the magnetic field dropped abruptly around 10 nT. Dal Lago et al. (2006) defined this point as the end of the ICME. They were not sure whether this ICME is an MC or not according to the criteria of Burlaga et al. (1981), because the direction of the magnetic field does not rotate smoothly. Cane and Richardson (2003) also detected one ICME not classified as MC at the date 21 October 08 : 00 UT - 22 October 07 : 00 UT 1999 with $V_{ICME} = 500$ km/s, $V_{max} = 580$ km/s, $B = 20$ nT and $V_T = 480$ Km/s.

452 As presented in the previous paragraph it is clear that during the period 20 – 26 October 1999 was not identified any magnetic cloud. In Figure 12, we show the values of spatio-temporal entropy as a function of the time for times series of IMF B_x , B_y , and B_z components in the solar wind from 20 – 26 October. All time the values of STE are different of zero, so the EI is also different from zero. This result helped to validate the EI to detect MC, because EI methodology can differentiate when an ICME is not classified as a MC, since the EI is zero only inside a MC.

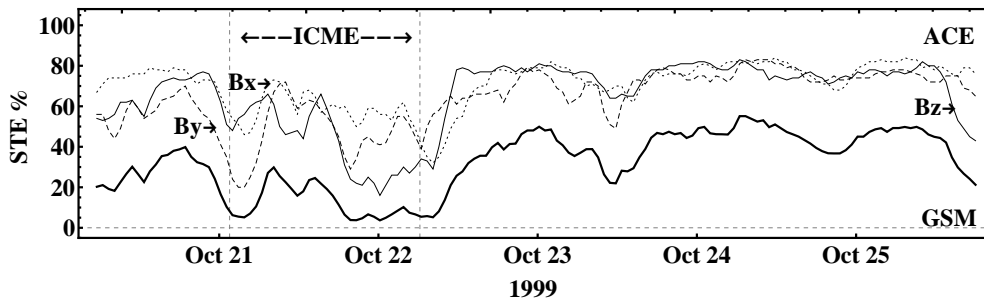


Figure 12: Values of spatio-temporal entropy on 20 – 26 October, 1999 as a function of the time for times series of IMF B_x , B_y and B_z components in the solar wind. The thick curve represents the Entropy Index (EI) calculated over the period analyzed.

457 *3.2.6. Identification by windowed STE method of 05-06 April 2010 MC event*

458 On 3 April 2010 the Sun launched a cloud of material, known as a coronal mass ejection (CME), in a direction that reaches the Earth. This CME was much faster than most of the CMEs seen recently, with a speed of at least 800 Km/s. The bulk of the CME passed south of Earth, but a piece of it hit the Earth's magnetosphere on April 5, causing a geomagnetic storm ($Dst_{min} = -73$ nT on 06 April at 15 : 00 UT). As a result bright auroras were seen around the world at higher latitudes.

463 This event was very recent and we wanted to use the technique to verify any possible MC occurrence. The ACE Magnetic Field Experiment data in level 2 (verified) were not available in April 2010 when the data were processed. It was only possible to obtain such data for 16 second average IMF in RTN and GSE coordinates via anonymous ftp, from Caltech⁵. For this reason, in Figure 13 the STE values are calculated for data in GSE coordinates.

⁵[ftp://mussel.srl.caltech.edu /pub/ace/browse/MAG16sec](ftp://mussel.srl.caltech.edu/pub/ace/browse/MAG16sec)

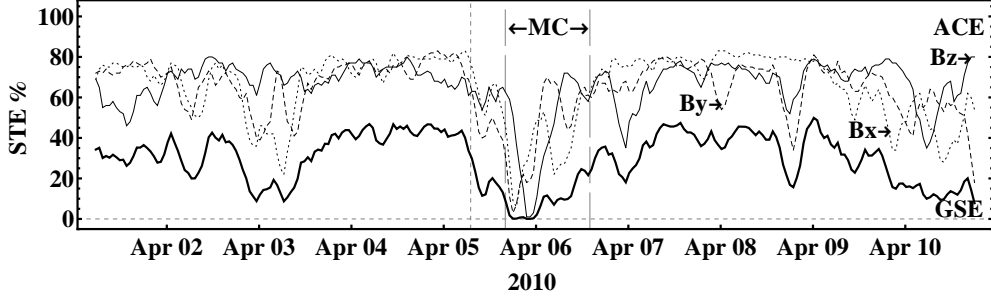


Figure 13: Values of spatio-temporal entropy on 01 – 11 April, 2010 as a function of the time for times series of IMF B_x , B_y and B_z components in the solar wind. The thick curve represents the Entropy Index (EI) calculated over the period analyzed. The MC is identified.

Figure 13 is similar to Figure 6 but for the period 01 – 10 April 2010 with GSE coordinates. We find minimum values of $STE = 1\%$ to B_z on 05 April at 21 : 33 : 20 and 22 : 26 : 40 UT respectively. The B_x and B_y components had STE values less than 10% on 05 April at 18 : 00 : 00 and 18 : 53 : 20 UT respectively. Then, the EI has a minimum values less than 1% on day 05 between 18 : 00 : 00 to 23 : 20 : 00 UT. Thus the EI detects a structure with characteristics of a magnetic cloud. The same method (MVA) explained in Huttunen et al. (2005) was used to find the boundaries of the cloud.

Table 6: Magnetic Cloud from 05 – 06 April 2010.

Year	Shock	MC, start	MC, stop
2010	05 April, 07 : 00	05 April, 16 : 00	06 April, 14 : 00

Figure 11(b) is similar to (a) but from 01 – 11 April 2010. On 05 April 2010, at 07 : 00 UT, the proton density $N_p = 2.8 \text{ cm}^{-3}$, proton temperature $T_p = 2.4 * 10^5 \text{ K}$, ratio of α /protons $= 7 * 10^{-2}$, proton speed $V_p = 564.5 \text{ km/s}$, magnetic field magnitude $B = 5.2 \text{ nT}$ and plasma beta $\beta = 0.9$. One hour later some parameters have an change $N_p = 7.98 \text{ cm}^{-3}$, $T_p = 5.5 * 10^5 \text{ K}$, α /protons $= 1.7 * 10^{-2}$, $V_p = 724.8 \text{ km/s}$, $B = 10.9 \text{ nT}$ and $\beta = 1.3$. It is easy to identify a shock because the velocity, density and magnetic field magnitude increases abruptly and we believe it is related to the arrival of an event to ACE. Eight hours latter than the time of the shock, at 16 : 00 UT, the plasma beta decreases to $\beta = 3.2 * 10^{-2}$, and it is the beginning of the magnetic cloud. The plasma beta minimum value were $\beta = 8.8 * 10^{-3}$ on 06 April at 12 : 00 UT. We used the magnetic field rotation confined to one plane, the plane of maximum variance ($B_x^* B_y^*$) to find the boundaries of the cloud (see Table 6). The MVA method gives the eigenvalue ratio $\lambda_2/\lambda_3 = 16$, the angle between the first and the last magnetic field vectors $\chi = 48^\circ$, the orientation of the axis $(\phi_C, \theta_C) = (33^\circ, -32.6^\circ)$, the direction of minimum variance $(\phi_{min}, \theta_{min}) = (129^\circ, 9^\circ)$ and eigenvalues $[\lambda_1, \lambda_2, \lambda_3] = [16.8, 3.6, 0.2]$. This MC has a flux-rope type NWS (see panel two and three in Figure 11 (b)) and the observed angular variation of the magnetic field is left-handed.

3.3. Correlation between the Windowed STE and the inclination of IMF

Following the same idea presented in subsection 2.3, we calculate the STE versus the trend angle. In Figure 3, we presented time series plot of Lorenz data file include in the VRA for four different trend angles. We mentioned earlier that the time series of magnetic clouds are not stationary, there is a trend. The linear least squares fitting technique is the simplest and most commonly applied form of linear regression and provides a solution to the problem of finding the best fitting straight line through a set of points and to obtain the equation of the line. The angle θ that a line makes with the positive x axis is closely related to the slope m via the inverse tangent function $\theta = \tan^{-1}(m)$. We applied the previous methodology to all IMF time series shown in the Figures 6, 7, 9, 10, 12. In other word, we separate all pairs of points formed by the trend angle θ and STE for the data.

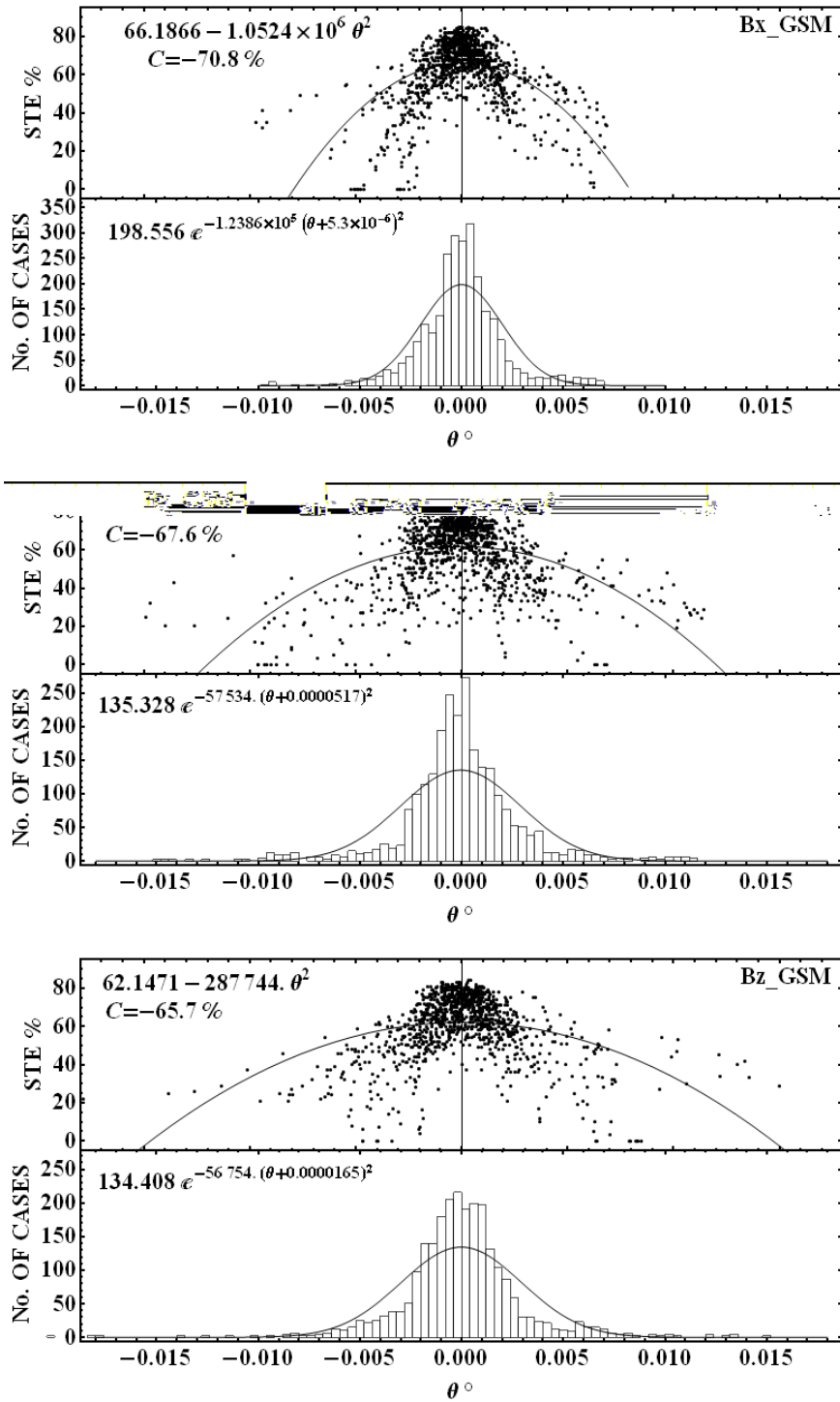


Figure 14: At top: Plot of STE versus θ to B_x , B_y and B_z components and a parabola fitted to the data. At bottom: The corresponding histogram in which a Gaussian distribution was fitted.

Figure 14 presents for the B_X , B_Y and B_Z components, at the top of each panel, the plot of STE versus θ for each magnetic component and a parabola fitted to the data, and at the bottom of each panel, the corresponding histogram, in which a Gaussian distribution was fitted. At the first panel in the figure, for B_X , from the STE versus θ , the correlation coefficient (a Pearson's correlation coefficient between two time series, STE vs θ) found was $C = -70.8\%$. If the variables tend to go up and down in opposition, with low values of one variable associated with high values of the other, the correlation coefficient will be negative (anti-correlation), as in our cases. The anti-correlation between the two parameters (STE and θ) gives the idea that the trend in the B_X series is responsible for the low values of STE. But the above idea is not totally true; because we have $STE \neq 0\%$ series with a larger trend, more separated points of the vertical line. The histograms help to see the distribution of the trend.

One response to these kinds of problems can be fluctuations in the signal. Sometimes, the trend in the records for a sheath region is bigger than the trend for a cloud, but the sheath has rapid fluctuations that changes the sign of the signal and the STE is not zero. Then the $STE = 0\%$ at magnetic clouds is related to the simultaneous occurrence of two factors: (1) the trend existing in the signal, (2) the analyzed variable (in this case, IMF B_x) has a more ordered dynamical behavior (*i.e.* few fluctuations) and higher degree of correlation between its time neighbors.

In Figure 14 the middle panel, for B_Y , and the bottom panel, for B_Z , present respectively the correlation coefficient (C) results of -67.6% and -65.7% . From the three panel, it is possible to see that B_z component has largest trend compared to the others two, but the reason is not know.

4. Conclusions

We dealt with time series of solar wind for a group of magnetic clouds in order to analyze the dynamical behavior of the IMF B_x , B_y and B_z components. The tool chosen to this study was the spatio-temporal entropy (called STE) method. From methodological considerations based on physical reasons, the STE was calculated from solar wind time windows with 2500 points corresponding to 11.11 hours of data. The results were significant and very promising. we found higher entropy values in the sheaths. MCs present zero STE values at least for one magnetic component. As not all the magnetic components have zero entropy at the same time, an useful technique was to create a standardization index, called Entropy Index (EI), to allow joining the STE results of the three variable (B_x , B_y , B_z). We studied in more detail the STE variations taking into account some days before and after to six selected events, in order to allow understanding and validating the analysis procedure. By this approach, the EI identified three new MCs in addition to the known MCs presented in previous tables from other researchers, and after the MVA method was used to calculate the boundaries easily.

The analyses developed in this work shows that:

- MCs have STE values lower than the ones for sheath region.
- The differences among the STE values for the three magnetic components in a MC give an idea about the anisotropy in the structure of some MCs. But this idea is still an open question to be better investigated.
- In MC the magnetic field strength is higher than the average, the magnetic field direction rotates smoothly through a large angle, then periods of MC have more trend than sheath region and "quiet" solar wind periods. The trend is the principal cause of the lower values of STE in the MC. Also, MCs are most structuredness than sheath and "quiet" solar wind.
- Using the EI and MVA method it is possible to identify all the magnetic clouds that arrive at spacecrafts.
- The entropy index (EI) proposed gets success as an auxiliary tool to identify magnetic cloud candidates and calculation of EI could be used in an automatic procedure of preliminary investigation or convenient warning.

Based on its skill to provide an objective analysis, the STE method can be seen as a valuable tool in the study of interplanetary phenomena such as the time localization of MCs.

537 5. Acknowledgments

538 This work was supported by CNPq (grants 309017/2007 – 6, 486165/2006 – 0, 308680/2007 – 3, 478707/2003,
539 477819/2003 – 6, 382465/01 – 6), FAPESP (grants 2007/07723 – 7) and CAPES (grants 86/2010 – 29). We are
540 grateful to V. E. Menconni (FAPESP 2008/09736 – 1) for their helpful computational assistance. The authors would
541 like to thank ACE Staff and WDC-Kyoto for the datasets used in this work. Ojeda G. A. would like to thank the
542 CAPES and CNPq for the PhD Scholarship Programme.

543 References

- 544 Bothmer, V., Schwenn, R., 1994. Eruptive prominences as sources of magnetic clouds in the solar wind. *Space Science Reviews* 70, 215.
545 Bothmer, V., Schwenn, R., 1998. The structure and origin of magnetic clouds in the solar wind. *Annales Geophysicae* 16, 1–24.
546 Burlaga, L., 1988. Magnetic clouds and force-free fields with constant alpha. *Journal of Geophysical Research* 93, 7217.
547 Burlaga, L. F., Sittler, E., Mariani, F., Schwenn, R., 1981. Magnetic loop behind an interplanetary shock: Voyager, helios and imp 8 observations.
548 *Journal of Geophysical Research* 86, 6673–6684.
549 Cane, H. V., Richardson, I. G., 2003. Interplanetary coronal mas ejections in the near-earth solar wind during 1996–2002. *Journal of Geophysical*
550 *Research* 108 (A4), 1156.
551 Carr, T. W., Schwartz, I. B., 1998. On measures of disorder in globally coupled oscillators. *Physica D* 115, 321–340.
552 Chartfield, C., Jul. 2003. *The analysis of time series an introduction*, sixth Edition. Chapman & Hall/CRC Texts in Statistical Science). Taylor &
553 Francis e-Library, 2009.
554 Dal Lago, A., Gonzalez, W., Balmaceda, A., L.E.A., V., Echer, E., Guarnieri, F., Santos, J., da Silva, M. R., de Lucas, A., Gonzalez, A., Schwenn,
555 R., Schuch, N., 2006. The 17–21 october (1999) solar-interplanetary-geomagnetic event: Very intense geomagnetic storm associated with a
556 pressure balance between interplanetary coronal mass ejection and a high-speed stream. *Journal of Geophysical Research* 111, A07S14.
557 Dasan, J., Ramamohan, T. R., Singh, A., Nott, P. R., 2002. Stress fluctuations in sheared stokesian suspensions. *Physical Review E* 66 (2), 021409.
558 Démoulin, P., Dasso, S., May 2009. Causes and consequences of magnetic cloud expansion. *Astronomy and Astrophysics* 498 (2), 551–566.
559 Eckmann, J., Kamphorst, S., Ruelle, D., 1987. Recurrence plots of dynamical systems. *Europhysics Letters* 4 (9), 973–977.
560 Facchini, A., Mocenni, C., Vinicio, A., 2009. Generalized recurrence plots for the analysis of images from spatially distributed systems. *Physica D*
561 238, 162–169.
562 Gosling, J., 1990. Coronal mass ejections and magnetic flux ropes in interplanetary space. In: Russel, C. T., Priest, E. R., Lee, L. C. (Eds.), *Physics*
563 *of Magnetic Flux Ropes*. AGU Geophys. Monogr., p. 343.
564 Huttunen, K. E. J., Bothmer, V., Koskinen, H. E. J., 2005. Properties and geoeffectiveness of magnetic clouds in the rising, maximum and early
565 declining phases of solar cycle 23. *Annales Geophysicae* 23, 1–17.
566 Klein, L. W., Burlaga, L. F., 1982. Interplanetary magnetic clouds at 1 au. *Journal of Geophysical Research* 87, 613–624.
567 Kolmogorov, A. N., 1958. A new metric invariant of transitive dynamical systems and automorphisms of lebesgue apacekol. *Dokl. Akad. Nauk*
568 *SSSR* 119, 861–864.
569 Lepping, R. P., Berdichevsky, D., 2000. Interplanetary magnetic clouds, sources, properties, modelling, and geomagnetic relationship. *Recent Res.*
570 *Devel. Geophys.* 3, 77–96.
571 Lepping, R. P., Jones, J. A., Burlaga, L. F., 1990. Magnetic field structure of interplanetary magnetic clouds at 1 au. *Journal of Geophysical*
572 *Research* 95, 11957.
573 Little, M. A., McSharry, P. E., J., R. S., Costello, D. A., Moroz, I. M., 2007. Exploiting nonlinear recurrence and fractal scaling properties for voice
574 disorder detection. *BioMedical Engineering OnLine*.
575 Ma, Y., Zhang, H., 2001. Detecting motion object by spatial-temporal entropy. In: *IEEE International Conference on Multimedia and Expo*, 2001.
576 pp. 265–268.
577 Nieves-Chinchilla, T., Hidalgo, M., Sequeiros, J., 2005. Magnetic clouds observed at 1 au during the period 2000–2003. *Solar Physics* 232, 105–
578 126, 10.1007/s11207-005-1593-5.
579 URL <http://dx.doi.org/10.1007/s11207-005-1593-5>
580 Ojeda, G. A., Calzadilla, A., Lazo, B., Alazo, K., Savio, S., 2005. Analysis of behavior of solar wind parameters under different imf conditions
581 using two nonlinear dynamics techniques. *Journal of Atmospheric and Solar-Terrestrial Physics* 67, 1859–1864.
582 Osherovich, V., Burlaga, L. F., 1997. Magnetic clouds. In: Crooker, N., Joselyn, J., Feynman, J. (Eds.), *Coronal Mass Ejection*. Vol. 99. AGU,
583 Washington, D. C., p. 157.
584 Peacock, J. A., Feb. 1983. Two-dimensional goodness-of-fit testing in astronomy. *Royal Astronomical Society* 202 (1983), 615–627.
585 Remya, R., Unnikrishnan, K., 2010. Chaotic behaviour of interplanetary magnetic field under various geomagnetic conditions. *Journal of Atmo-*
586 *spheric and Solar-Terrestrial Physics* 72 (9–10), 662–675.
587 URL <http://www.sciencedirect.com/science/article/B6VHB-4YMY76K-1/2/2892ca567726bd7b3108fb5957825c80>
588 Renyi, A., 1959. On a theorem of erdos and its application in information theory. *Mathematica* 1, 341–344.
589 Richardson, I. G., Cane, H. V., 1995. Regions of abnormally low proton temperature in the solar wind (1965 – 1991) and their association with
590 ejecta. *Journal of Geophysical Research* 100, 23397.
591 Schwenn, R., 2006. Space weather: The solar perspective. *Living reviews in solar physics* 3 (2), 1–72.
592 Shannon, C., Weaver, W., Jul. 1948. The mathematical theory of communication. *The Bell System Technical Journal* 27, 379–423, 623–656.
593 Sinai, Y. G., 1959. On the concept of entropy of a dynamical system. *Dokl. Akad. Nauk SSSR* 124, 768–771.
594 Sonnerup, B., Cahill, L., 1967. Magnetopause structure and attitude from explorer 12 observations. *Journal of Geophysical Research* 72, 171.
595 Takens, F., 1981. Detecting strange attractors in turbulence. *Lecture Notes in Mathematics*, 366–381.

596 Tsurutani, B., Gonzalez, W., Tang, F., Akasofu, S., Smith, E., 1988. Origin of interplanetary southward magnetic fields responsible for major
597 magnetic storms near solar maximum (1978-1979). *Journal of Geophysical Research* 93, 8519–8531.
598 Webber, C. L., Zbilut, L. P., 1994. Dynamical assessment of physiological systems and state using recurrence plot strategies. *Journal of Applied*
599 *Physiology* 76, 965–973.
600 Zbilut, L. P., Webber, C. L., 1992. Embeddings and delays as derived from quantification of recurrence plots. *Physics Letters A* 171, 199–203.
601 Zhang, G., Burlaga, L. F., 1988. Magnetic clouds, geomagnetic disturbances and cosmic ray decreases. *Journal of Geophysical Research* 88, 2511.
602 Zwickl, R., Asbridge, J., Bame, S., Feldman, W., Gosling, J., Smith, E., 1983. Plasma properties of driver gas following interplanetary shocks
603 observed by isee-3. In: Neugebauer, M. (Ed.), in *Solar Wind Five*. Vol. 2280. NASA Conf. Publ., p. 711.